Volume 1 | Number 1 | Jan 2013 | Pages 1–100

Nanoscale

www.rsc.org/nanoscale

ROYAL SOCIETY OF CHEMISTRY

ROYAL SOCIETY OF CHEMISTRY

www.rsc.org/nanoscale

Stable J-aggregation enabled dual photoacoustic and fluorescence nanoparticles for intraoperative cancer imaging

Mojdeh Shakiba,[‡a,b][⊥] Kenneth K. Ng, [‡a,c] Elizabeth Huynh,[a,b] Harley Chan,[a, e] Danielle M. Charron, [a,c] Juan Chen,[a] Nidal Muhanna,[a] F. Stuart Foster,[b,d] Brian C. Wilson[a,b] and Gang Zheng[a,b,c]*

[a]Princess Margaret Cancer Centre and Techna Institute, University Health Network, Toronto, ON, Canada
[b]Department of Medical Biophysics, University of Toronto, Toronto, ON, Canada
[c]Institute of Biomaterials and Biomedical Engineering, Toronto, ON, Canada
[d]Sunnybrook Research Institute, Toronto, ON, Canada
[e]Guided Therapeutics, TECHNA Institute, University Health Network, Toronto, ON, Canada

[‡]These authors contributed equally to this work
[⊥]Present Address: Weill Cornell Medicine, Department of Physiology, Biophysics and Systems Biology, New York, NY, USA

*All correspondence can be sent to gang.zheng@uhnres.utoronto.ca

ABSTRACT

J-aggregates display nanoscale optical properties which enable their use in fluorescence and photoacoustic imaging applications. However, control over their optical properties in an *in vivo* setting is hampered by the conformational lability of the J-aggregate structure in complex biological environments. J-aggregating nanoparticles (JNP) formed by self-assembly of bacteriopheophorbide-lipid (Bchl-lipid) in lipid nanovesicles represents a novel strategy to stabilize J-aggregates for *in vivo* bioimaging applications. We find that 15 mol % Bchl-lipid embedded within a saturated phospholipid bilayer vesicle was optimal in terms of maximizing Bchl-lipid dye loading, while maintaining a spherical nanoparticle morphology and retaining spectral properties characteristic of J-aggregates. The addition of cholesterol maintains the stability of the J-aggregate absorption band for up to 6 hours in the presence of 90% FBS. In a proof-of-concept experiment, we successfully applied JNPs as a fluorescence contrast agent for real-time intraoperative detection of metastatic lymph nodes in a rabbit head-and-neck cancer model. Lymph node metastasis delineation was further verified by visualizing the JNP within the excised lymph node using photoacoustic imaging. Using JNPs, we demonstrate the possibility of using J-aggregates as fluorescence and photoacoustic contrast agents and may potentially spur the development of other nanomaterials that can stably induce J-aggregation for *in vivo* cancer bioimaging applications.

INTRODUCTION

Organic dyes that assemble with short- and long- range order can display optical properties distinct from the individually-dispersed monomer. The assembly of dyes which causes a red-shift, intensi-

fication and narrowing of the absorption band has been named the J-aggregate, after Edwin Jelley, who was credited for its initial characterization[1, 2]. Since then, research on these nanoscale assemblies has flourished due to their interesting optical properties including third order non-linearity[3, 4], superradiance[5, 6] and conformation-dependent optical spectra[7]. J-aggregates have found commercial applications as spectra sensitizers in photographic film development[8] and have been used as fluorescent sensors of mitochondrial membrane potential in biomedical research[9].

There have been relatively few applications of J-aggregates for *in vivo* imaging despite their unique optical properties. This challenge can be attributed to the dependence of the optical properties on the geometry of the interacting dyes involved in the J-aggregate. These interactions can be disrupted in biological solutions where complex mixtures of proteins, lipids and salts can alter the packing arrangement of the J-aggregate. This is highlighted by indocyanine green (ICG), a FDA-approved near-infrared dye that exhibits concentration-dependent J-aggregation[10]. ICG switches from an aggregated to a monomeric state upon binding to serum albumin protein leading to concomitant changes in absorption and fluorescence[11]. One way to surmount this challenge is to induce assembly of J-aggregates within the stabilizing environment of a structured nanomaterial. Examples of this strategy include assembly of J-aggregates within DNA[12], collagen proteins[13] and lipid bilayers[14-16].

J-aggregate forming nanoparticles (JNP) are 100 nm lipid-based nanovesicles in which a J-aggregate forming bacteriopheophorbide-lipid (Bchl-lipid) dye (Fig. S1) is inserted. We recently showed that assembly of these dyes into lipid membranes results in a 75nm bathochromic shift in absorption as well as narrowing and intensification of the lowest energy absorption band. We found that by varying the amount of thermal energy in the aqueous system, we could induce changes in the aggregation state of Bchl-lipid. This flexibility in the assembly's conformational state opened up the possibility of sensing temperature changes *in vivo*[17]. To further expand on this platform for theranostic applications *in vivo*, we were motivated to study the influence that local membrane environment as well as dye loading percentage has on the optical and morphological properties of JNPs. Here, we report our findings on the influence of membrane environment on Bchl-lipid assembly in JNPs and investigate their spectral attributes in the context of contrast-enhanced photoacoustic and fluorescence imaging. Lastly, we investigate the application of JNPs for fluorescence-guided metastatic lymph node surgical resection[18] and *ex vivo* photoacoustic imaging validation in a rabbit model of head and neck cancer.

EXPERIMENTAL SECTION

Synthesis

Bacteriopheophorbide (Bchl)-lipid was synthesized as described by Lovell et al[19]. All nanoparticles were made by dispersion of Bchl-lipid, 1,2-dipalmitoyl-sn-glycero-3-phosphoethanolamine-N-[methoxy(polyethylene glycol)-2000] (DPPE-PEG(2000)), and either 1,2-dipalmitoyl-sn-glycero-3-phosphocholine (DPPC) or 1-palmitoyl-2-oleoyl-sn-glycero-3-phosphocholine (POPC) in chloroform, followed by evaporation under nitrogen to form a lipid film. These films were then hydrated in phosphate-buffered saline (PBS) and subjected to ten freeze-thaw cycles. In order to form a monodisperse population of nanoparticles, the solution was extruded with a 100 nm polycarbonate membrane at 65°C. Nanoparticles were stored under argon at 4°C until used for experiments.

Characterization

Size distribution was measured by dynamic light scattering using a Nanosizer ZS90 (Malvern Instruments) and the Z-average size measurement was calculated from the acquired data. Morphology was characterized by Hitachi H-7000 transmission electron microscopy (TEM), with 2% uranyl acetate negative staining. UV/visible absorption spectra were obtained in PBS and in methanol (MeOH) using the Cary 50 UV-visible spectrophotometer (Agilent, Mississauga, ON). Fluorescence measurements were carried out using a Fluoromax-4 spectrofluorometer (Horiba Scientific, NJ).

Tumor cell line propagation

The tumor cell line is maintained in small pieces that are frozen at -80°C. Tumor cells were propagated by injecting 500 μL of VX-2 tumor into the quadricep muscle and harvested after approximately 3 weeks. The harvested tumor was placed into Hanks balanced salt solution (HBSS) in a sterile 100 mL container. Prior to tumor induction in rabbits, the tumor pieces were thawed and cut into small pieces using a sterile scalpel and subsequently placed on to a 70-μm-cell strainer sitting on a 50 mL tube (BD Falcon). A syringe plunger was used to mince the cells and ~500 μL HBSS was used to suspend the cells in a strainer. These cells were subsequently used for tumor induction.

Animal Studies

All animal experiments were approved by the institutional Animal Care Committee of the University Health Network. A pre-clinical head and neck cancer model was developed using New Zealand white (NZW) rabbits (Charles River, Washington, Massachusetts) weighing 2.5-3.0 kg[18]. Briefly, the NZW rabbit was injected with 300 μL of the prepared VX-2 cell suspension (5×10^6 cell/mL) into the buccinator muscle under general anesthesia. Tumor development was closely monitored by physical examination. Two weeks after inoculation, the tumor reached size 1.5 cm and at least one cervical lymph

node metastases was generated. These finding were confirmed by physical palpation and computed tomogra-phy (CT) imaging.

Fluorescence imaging session

Under general anesthesia, the rabbit was subcutaneously injected with 750 μL of 15% Bchl-lipid JNP (200μM dye concentration) at four points around the tumor. Baseline pre-operative fluorescence imaging was performed before JNP injection to account for the background signal contribution. Fluorescence imaging devices employed in the study were the PINPOINT and SPY system (Novadaq Technologies Inc., Mississauga, ON, Canada). The PINPOINT system was designed for endoscopic usage and possesses a laser emitting at 808 nm. The SPY system was designed for open field procedure with an excitation laser wavelength 806 nm. Usage of both systems enabled the generation of white light and fluorescence composite images.

Fluorescence images of JNPs were captured after 1 hr to ensure adequate drainage to surrounding lymph nodes. A skin incision was subsequently made and the skin flap was raised where the metastatic lymph node was exposed. Fluorescence images were captured to confirm that the metastatic lymph node of interest was connected and drained from the tumor. The entire lymph node was subsequently removed for hyperspectral fluorescence and photoacoustic imaging. Control lymph nodes at a distant site were also collected for comparison. Lastly, the rabbit was euthanized under deep anesthesia (5% isoflurane) using 1.5 mL potassium chloride (149 mg/mL) administered intravenously.

Ex vivo **hyperspectral fluorescence and photoacoustic imaging**

Tissues were imaged by hyperspectral imaging using the near-infrared filter set (excitation: 735±25nm; emission: 800nm longpass) (Perkin-Elmer, Waltham, MA). Image cubes were captured at 500ms exposure time while scanning from 780-900nm at 10nm intervals. The fluorescence signal originating from the peak at 820nm was unmixed from the background and overlaid with a white-light reflectance image. For photoacoustic imaging, tissues were covered with ultrasound gel and imaged using the Vevo 2200 photoacoustic scanner (Visualsonics, Fuji-Film, ON) equipped with the LZ550 55MHz photoacoustic transducer. Spectral and 3D scans of the lymph node were captured at predetermined wavelengths ranging from 680 – 900nm. For 3D reconstruction, the photoacoustic signal intensity at 875 nm was taken as endogenous background and subtracted from 824nm.The transformed data was overlaid with the simultaneously acquired ultrasound B-mode image.

RESULTS AND DISCUSSION

Influence of membrane fluidity on J-aggregation

In nature, Bchl *a* is known to form J-aggregates within the light-harvesting complex of various types of photosynthetic bacteria[20, 21]. The formation of Bchl *a* J-aggregates in such complexes, however, is dependent on the rigid protein scaffolds and membrane lipids that surrounds them, which in turn dictate the orientation and the relative proximity of the dye molecules and thus their ability to coherently couple[20]. With JNPs formed from a mixture of Bchl-lipid and a host lipid, we sought to determine the role of host lipid membrane fluidity in supporting the formation of J-aggregates by varying the degree of saturation of the host lipid. Saturated lipids form a more rigid membrane than unsaturated lipid. We found that in the presence of the saturated phospholipid, DPPC, J-aggregation was independent of Bchl-lipid content, with the J-aggregate absorption peak at 824 nm observed in as low as 5 mol % Bchl-lipid (Fig 1A). On the other hand, in the presence of an unsaturated host phospholipid, POPC, J-aggregation was found to be dependent on the molar percentage of Bchl-lipid in the formulation (Fig 1B). At 5%mol Bchl-lipid content, no J-aggregation was observed in presence of an unsaturated host lipid, with the absorption spectrum being the same as that of the monomeric Bchl-lipid dye. Increasing the Bchl-lipid content resulted in the emergence of the J-aggregate peak, with the intensity of this peak increasing relative to that of the monomeric peak (Fig 1B). The high membrane fluidity in an unsaturated host lipid results in dispersion of Bchl-lipid molecules and hence the presence of the monomeric peak. Increasing the Bchl-lipid content, however, overcomes this effect, as a greater percentage of the lipid content is able to form J-aggregates. In a saturated host lipid, the rigidity of the membrane allows for formation of J-aggregates even at low Bchl-lipid content (Fig 1B). Comparing the ratio of the J-aggregate absorption band to the monomeric band (A824nm/A750nm), indicated that the saturated host lipid provides a more favorable environment for Bchl-lipid J-aggregation than does the unsaturated host, regardless of the amount of Bchl-lipid present (Fig 1C). Taken together, these results indicate that membrane fluidity plays an important role in the ordered J-aggregation process in Bchl-lipid dyes. We focused the remaining studies on JNPs formed with DPPC, as it robustly supported the formation of J-aggregates.

Influence of Bchl-lipid content on spectral and morphological properties in JNPs

We next studied the effect of Bchl-lipid content on the spectral and morphological properties of JNPs. We examined the line-width and bathochromic shift of the Q_y absorption band, as well as the Stokes shift and fluorescence quenching percentage as a function of Bchl-lipid content. Full-width at half-maximum measurements (FWHM) showed that the aggregating sample absorption peak was approximately 1.8 times more narrow than the comparable monomeric dye absorption, which had a FWHM of 40nm (Fig 2A). JNPs made with DPPC were found to display a bathochromic absorption

shift of ~75 nm independent of the Bchl-lipid loading (Fig 2B). Taken together, these results show that between the concentrations of 5-20 mol % Bchl-lipid, there was no differences in the absorption band properties in each sample.

Comparing the Stokes shift and fluorescence quenching, it was found that increasing the loading of Bchl-lipid increased the Stokes shift slightly from 1 nm to 3 nm (Fig 2C). At the same time, fluorescence self-quenching was only found to increase moderately from 1-fold (5 mol % Bchl-lipid) to 2-fold (20 mol % Bchl-lipid) (Fig 2D). This is an interesting observation since previously published studies on porphyrin-lipid nanovesicles showed self-quenching ranging from ~2-fold and 110-fold for the 5% and 20% porphyrin-lipid loading, respectively[19]. This reduced self-quenching is a property of J-aggregates and can potentially be useful in near-infrared (NIR) fluorescence imaging applications.

To study the influence of Bchl-lipid loading on vesicle morphology, we varied the loading of the dye and examined light scattering and transmission electron microscope (TEM) images of the vesicles after high-pressure lipid extrusion. The calculated z-average diameter varied between 100-150nm but without a discernable trend (Fig 3A). Studies of morphology by TEM showed that nanovesicles remained spherical up to 20% (Fig 3B). To determine the effect of storage on the morphology of JNPs, 15% and 20% JNPs were stored at 4°C for 7 days. The 20 mol % formulation formed more cylindrical structures after storage than the 15 mol % sample (Fig 3C). These results could potentially be explained by annealing of the Bchl-lipid aggregates upon storage at low temperature. Due to the posited head-to-tail packing requirements of ordered J-aggregation[22], annealing of oligomers could lead to formation of structures which cannot conform to the geometry required for vesicle formation.

In addition to storage stability and morphology, we were also interested in examining stability of JNPs under physiological conditions. We formed JNPs samples containing 15% Bchl-lipid (JNP15) and 40% cholesterol. Addition of cholesterol to lipid membranes has been shown to increase stability in physiological environments[23]. Addition of cholesterol did not change the absorption arising from the J-aggregation of Bchl-lipid dyes (data not shown). Using the intensity of the 824-nm J-aggregation band, we examined the stability of J-aggregation at various serum incubation concentrations over time (Fig. 4). We found that incubating JNPs with 10% and 50% fetal bovine serum (FBS) did not alter the intensity of the absorption band over the 2-day study period, indicating the particle remained stable. Incubation with 90% FBS resulted in a decrease in the J-aggregate band by 35% and 44% after 24 and 48 hrs, respectively (p-value < 0.05). However, since JNPs were found to be stable between 6 to 24 hr in 90% FBS, they were deemed suitable for use as *in vivo* imaging agents.

Intraoperative lymph node resection in head-and-neck cancer animal model

Based on the results of the previous experiments, we concluded that the JNP15 made with DPPC was the optimal candidate for further *in vivo* testing as demonstrated by a large red-shifted absorption, only 2-fold fluorescence self-quenching and retained its morphology upon extended storage. We proceeded to investigate the performance of the JNP15 as a contrast agent for lymph node resection using intraoperative fluorescence imaging in a rabbit head-and-neck cancer model.

Surgery is a common strategy for treating head and neck cancer tumors. However, the presence of metastasis in downstream drainage lymph nodes is an indicator of poor survival and may increase the risk for distant metastasis[24, 25]. For this reason, the ability to determine and eliminate nearby diseased lymph nodes in the pre-operative or the operative stage is critical to reduce the risk of metastatic cancer recurrence. We postulated that the large absorption cross-section and fluorescence properties of J-aggregates could be used to identify diseased lymphatic tissue near the primary tumor. In a proof-of-concept experiment, we tested whether JNP15 can be used intraoperatively to facilitate diseased lymph node detection, removal and confirmation.

A VX-2 buccal tumour bearing rabbit (n=1) was injected with JNP15 intradermally at four locations around the primary tumor. JNPs were allowed to drain to nearby lymph nodes over a period of 1 hr. The peritumoral area was visualized using an intraoperative fluorescence endoscope equipped with either the 806nm or 808nm laser. While the excitation light sources did not couple efficiently to the absorption band of the JNPs, it was nonetheless suitable for fluorescence excitation. Images were collected in either the fluorescence or the combined white light/fluorescence mode using the Pinpoint® and Spy® systems, respectively. After 1 hr, a fluorescent signal could be observed over a region of the skin distinct from that formed at the injection site. A skin flap was raised and the fluorescent lymph node was visualized (Fig 5A). The diseased lymph node was removed along with nearby healthy lymph nodes and salivary glands. These tissues were subjected to hyperspectral fluorescence and photoacoustic imaging. Despite suboptimal excitation, clear fluorescent images were captured and allowed for rapid determination of the distal lymph node. This can be attributed to the low fluorescence background in the absence of the contrast agent.

Ex vivo **fluorescence and photoacoustic imaging confirmation**

Ex vivo hyperspectral fluorescence imaging of the resected tissue showed signal originating from one focal region of the lymph node (Fig 5B). Emission spectra collected in this area showed a fluorescence maximum at 820nm, corresponding to the near-infrared emission of JNPs. Endogenous tissue background fluorescence in this region of the spectrum is at a minimum. While near-infrared fluores-

cence is a powerful technique for intraoperative imaging due low background signal and high sensitivity, depth information is lost due to the scattering of emitted photons which limits the spatial resolution of this technique at depth. Photoacoustic imaging in comparison, relies on the detection of ultrasound generated by the pressure waves emanating from the thermoelastic expansion of heated tissues. This periodic heating of tissue is caused by the molecular process of absorption and vibrational relaxation of either exogenous or endogenous tissue absorbers under illumination. J-aggregates that display red-shifted absorption in the near-infrared can be used as photoacoustic contrast agents due the enhanced absorption of the aggregate compared to the individual monomers. Excised lymph nodes from rabbits were scanned using photoacoustic imaging (Fig 5C). The photoacoustic spectrum originating from the metastatic lymph nodes showed peaks at 760nm and at 824nm. The signal at 760nm can be attributed to background photoacoustic signal from hemoglobin. Scans of the untreated salivary gland at a distant site showed the presence of this signal (Fig S2A). The signal at 824nm corresponds to the photoacoustic signal originating from the J-aggregate, which can be resolved at depths as great as 4mm. The spatial distribution of this 824nm signal can be observed in the upper half of the cross-sectional image through the tissue (Fig 5C). Given the narrowness of the absorption band from JNP15 (~25nm) and the invariability of hemoglobin's photoacoustic spectrum between 824 and 875nm (Fig S2B), it is possible to separate the hemoglobin contribution to the photoacoustic signal by taking the difference between signal intensity at 824 nm and 875 nm. Rendering the individual slices after doing this transformation results in a clear image showing the location of the JNP signal within the lymphatic tissue (Fig 5D). While the photoacoustic contrast enhancement of JNPs was only demonstrated *ex vivo*, with the suitable instrumentation, this strategy could conceivably be adapted for intraoperative detection of metastatic lymph nodes.

CONCLUSION

In summary, the fluorescence and intense absorption properties of near-infrared-absorbing J-aggregates enable their application for *in vivo* imaging. However, utility of these aggregates has been hampered by the dependence of their optical properties on their packing arrangement; which in turn is heavily influenced by their factors such as dye concentration and its surrounding environment. Embedding J-aggregating Bchl-lipid dyes within the membrane of saturated phospholipid nanovesicles overcomes this limitation by providing a scaffold for the stable assembly of the dye aggregates. We find that JNPs can be used as fluorescent nanoparticles for intraoperative imaging of potentially metastatic drainage lymph nodes near primary buccal tumors in a rabbit model of head and neck cancer. As nanoparticles, JNPs naturally have the additional capability of targeting tumor cell surface receptors upon bioconjugation with targeting ligands. With sufficient time allotted for non-specific washout in lymphatic tissues, it may eventually be possible to detect metastatic cancer cells within lymph nodes. Furthermore, due to the conformation-dependent nature of the J-aggregate spectra, it may be possible to program JNPs to respond to tumor-specific inputs and report them through alterations in optical spectra. Overall, we anticipate that the unique optical properties JNPs, together with their organic and biocompatible nature, will prove to be an interesting avenue of future investigation into contrast enhanced imaging applications.

ACKNOWLEDGMENT

REFERENCES

1.   E. E. Jelley, *Nature*, 1937, **139**, 2.
2.   E. E. Jelley, *Nature*, 1936, **138**, 2.
3.   Y. Wang, *J. Opt. Soc. Am. B*, 1991, **8**, 981-985.
4.   F. C. Spano and S. Mukamel, *Phys. Rev. A*, 1989, **40**, 5783-5801.
5.   H. Fidder, J. Knoester and D. A. Wiersma, *Chem. Phys. Lett.*, 1990, **171**, 529-536.
6.   F. C. Spano and S. Mukamel, *J. Chem. Phys.*, 1989, **91**, 683-700.
7.   A. Eisfeld and J. S. Briggs, *Chem. Phys.*, 2006, **324**, 376-384.
8.   B. Trösken, F. Willig, K. Schwarzburg, A. Ehret and M. Spitler, *Adv. Mat.*, 1995, **7**, 448-450.

9.   M. Reers, T. W. Smith and L. B. Chen, *Biochemistry*, 1991, **30**, 4480-4486.
10.   F. Rotermund, R. Weigand and A. Penzkofer, *Chem. Phys.*, 1997, **220**, 385-392.
11.   J. Bongsu, V. I. Vullev and B. Anvari, *IEEE J. Sel. Top. Quantum Electron.*, 2014, **20**, 149-157.
12.   M. Wang, G. L. Silva and B. A. Armitage, *J. Amer. Chem. Soc.*, 2000, **122**, 9977-9986.
13.   A. S. Tatikolov and I. G. Panova, *High Energy Chem.*, 2005, **39**, 232-236.
14.   T. Seki, K. Ichimura and E. Ando, *Langmuir*, 1988, **4**, 1068-1069.
15.   H. Hada, R. Hanawa, A. Haraguchi and Y. Yonezawa, *J. Phys. Chem.*, 1985, **89**, 560-562.
16.   G. C. H. Mo and C. M. Yip, *Langmuir*, 2009, **25**, 10719-10729.
17.   K. K. Ng, M. Shakiba, E. Huynh, R. A. Weersink, Á. Roxin, B. C. Wilson and G. Zheng, *ACS Nano*, 2014, **8**, 8363-8373.
18.   N. Muhanna, L. Cui, H. Chan, L. Burgess, C. S. Jin, T. D. MacDonald, E. Huynh, F. Wang, J. Chen, J. C. Irish and G. Zheng, *Clin. Cancer Res.*, 2015, DOI: 10.1158/1078-0432.ccr-15-1235.
19.   J. F. Lovell, C. S. Jin, E. Huynh, H. Jin, C. Kim, J. L. Rubinstein, W. C. Chan, W. Cao, L. V. Wang and G. Zheng, *Nat. Mater.*, 2011, **10**, 324-332.
20.   G. McDermott, S. M. Prince, A. A. Freer, A. M. Hawthornthwaite-Lawless, M. Z. Papiz, R. J. Cogdell and N. W. Isaacs, *Nature*, 1995, **374**, 517-521.
21.   R. J. Cogdell, T. D. Howard, N. W. Isaacs, K. McLuskey and A. T. Gardiner, *Photosynth. Res.*, 2002, **74**, 135-141.
22.   T. Seki and K. Ichimura, *J. Phys. Chem.*, 1990, **94**, 3769-3775.
23.   C. Kirby, J. Clarke and G. Gregoriadis, *Biochem. J.*, 1980, **186**, 591-598.
24.   B. C. Lucey, J. W. Stuhlfaut and J. A. Soto, *Radiographics*, 2005, **25**, 351-365.
25.   V. Pagliarulo, D. Hawes, F. H. Brands, S. Groshen, J. Cai, J. P. Stein, G. Lieskovsky, D. G. Skinner and R. J. Cote, *J. Clin. Oncol.*, 2006, **24**, 2735-2742.
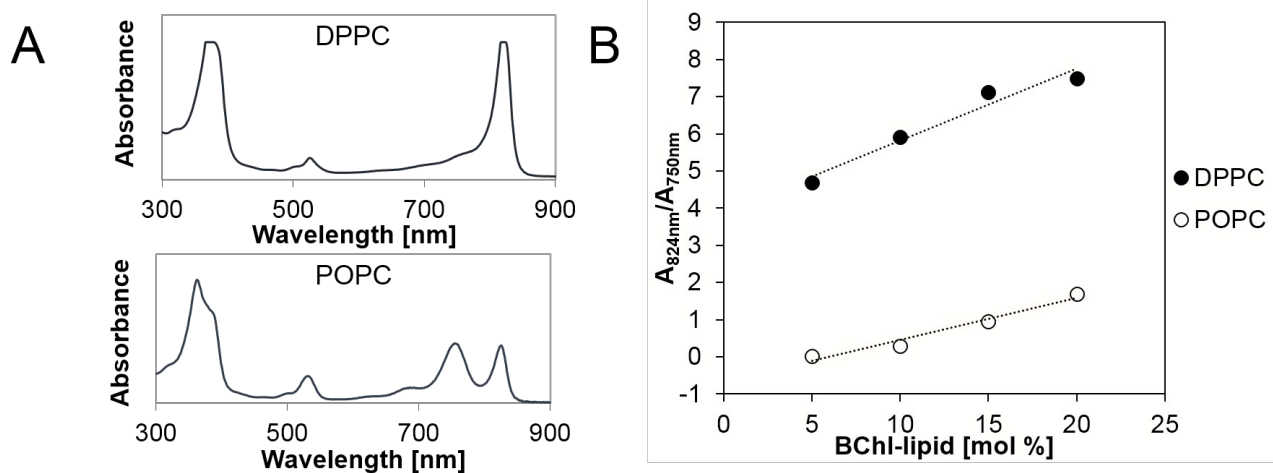
FIGURES

Fig. 1. Influence of membrane fluidity on J-aggregation in JNPs (A) Representative absorption spectra of 15 mol% Bchl-lipid samples formed in DPPC (top) or POPC (bottom) lipid vesicles. (B) Ratio of absorption between J-aggregate band (824nm) and monomer band (750nm). Lipid vesicles prepared with saturated phospholipid DPPC shows greater J-aggregate formation than unsaturated POPC vesicles at all Bchl-lipid ratios.
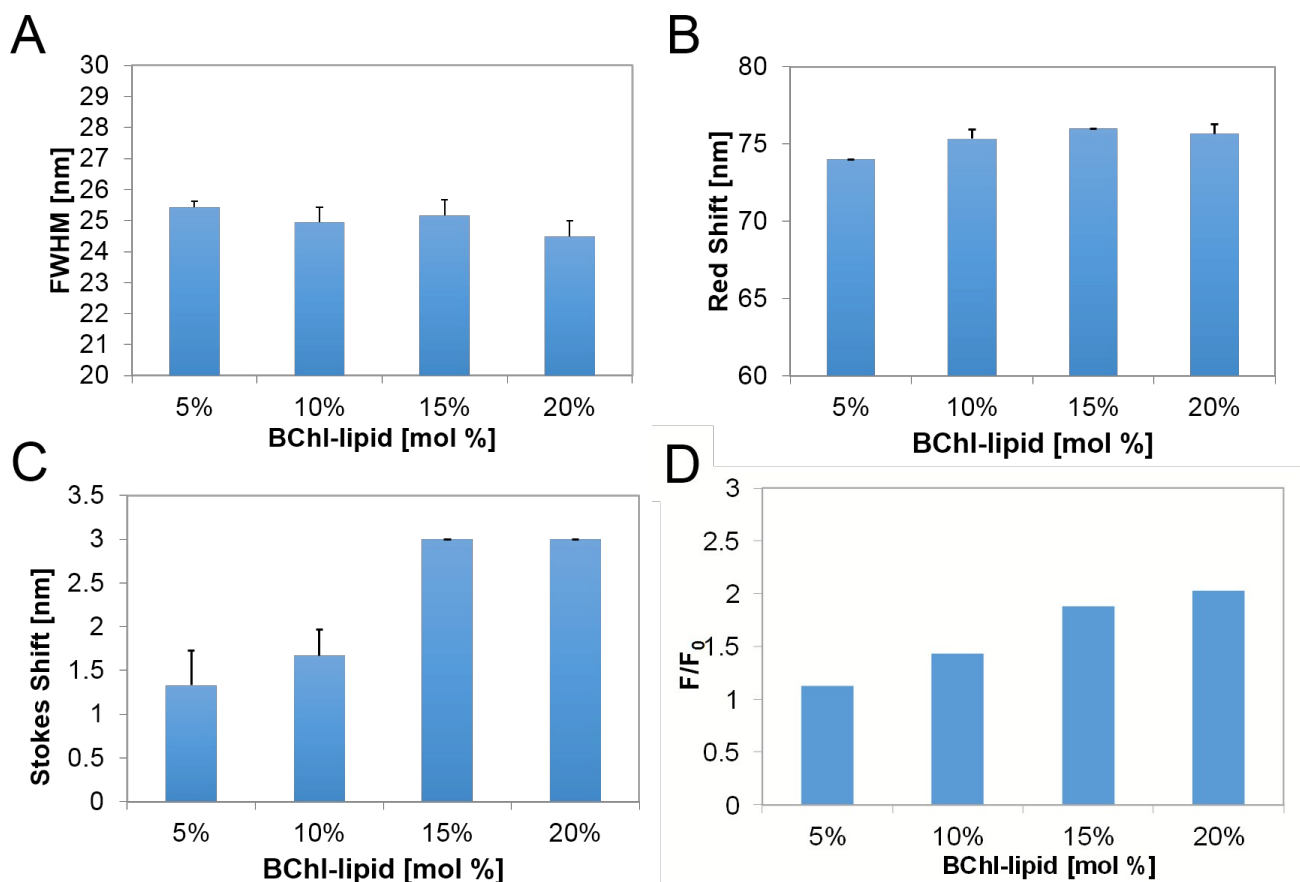
Fig. 2. Absorption and fluorescence properties of JNPs prepared with DPPC at various amounts of Bchl-lipid. All data correspond to the average ± s.d. of three replicates. (A) Full-width at half-maximum of the J-aggregate absorption band (peak = 824nm). (B) Extent of the red shift in the J-aggregate absorption band relative to the position of the monomeric absorption at 750nm. (C) Fluorescence Stokes shift at various Bchl-lipid loading ratios. (D) Fluorescence self-quenching as a function of Bchl-lipid loading.
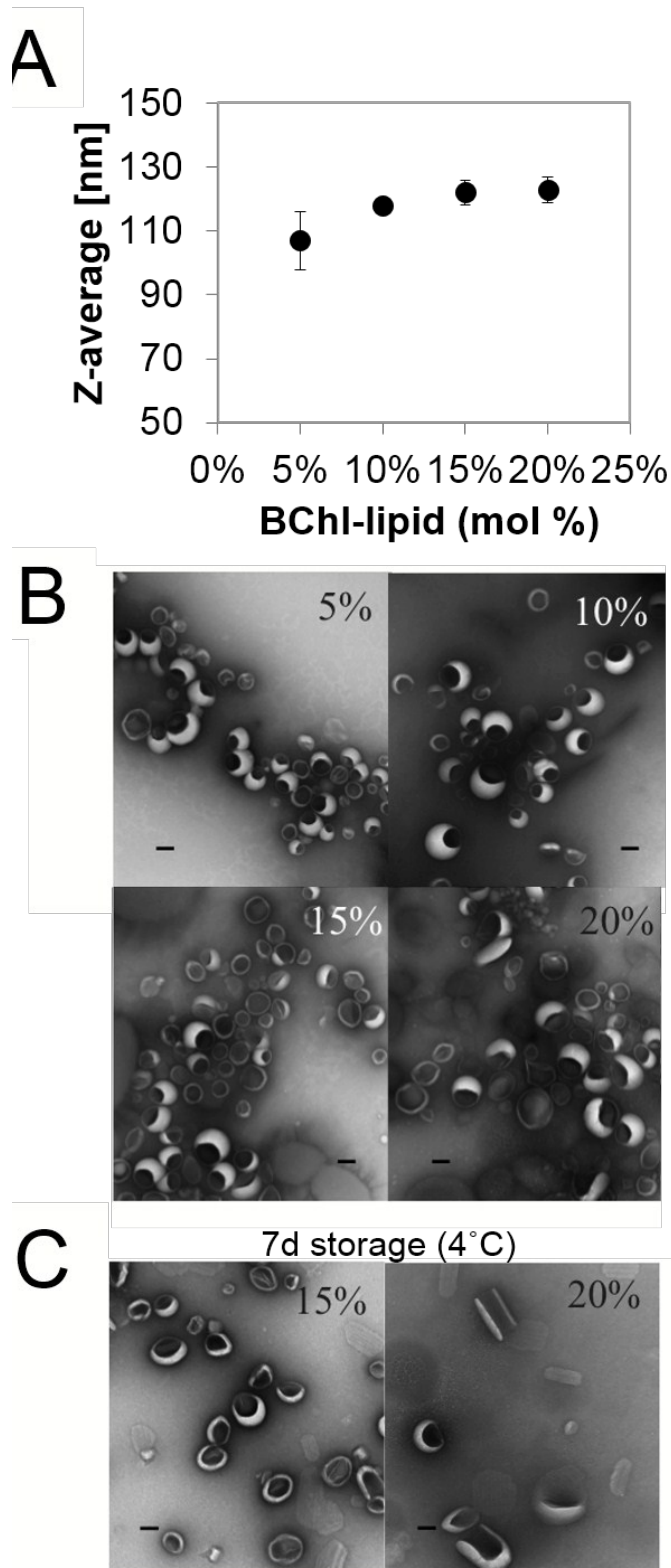
Fig. 3. Size and morphological property changes of BChl-lipid at various loading (mol %) in DPPC lipid membranes (A) Z-average diameter ± s.d. of three replicates measured using dynamic light scattering , (B) nanovesicle TEM morphology as function of loading %. (C) TEM morphology after storage for 7d at 4°C results. All scale bars represent 100nm.
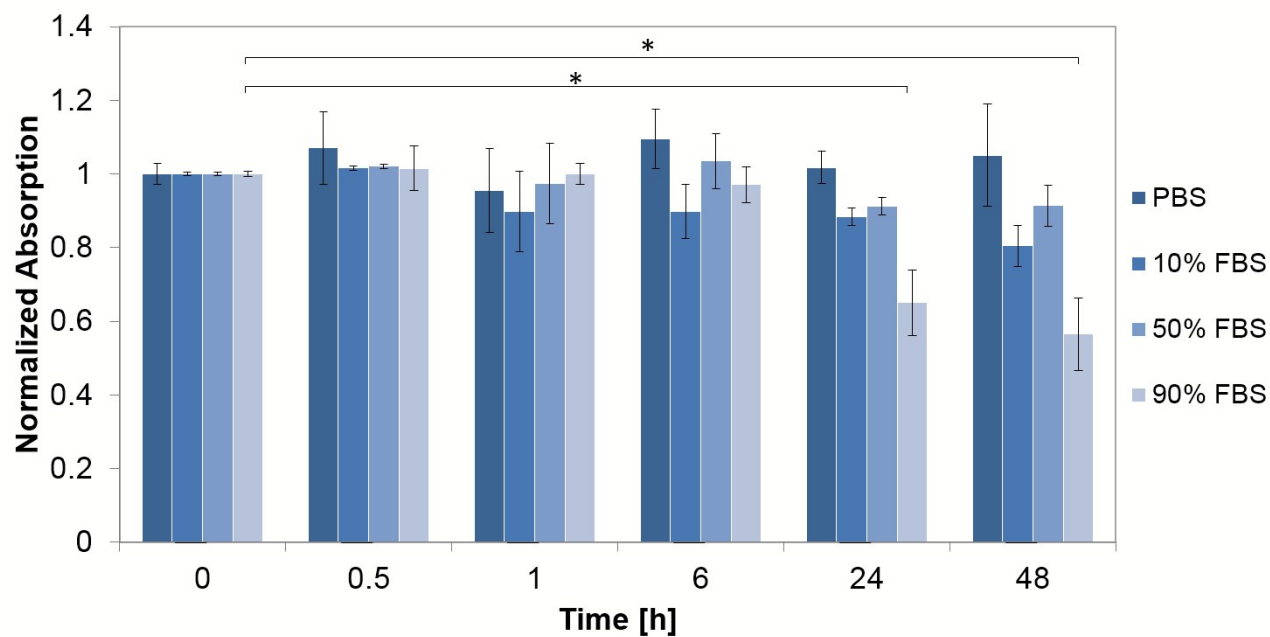
Fig. 4. Stability of 15% mol Bchl-lipid JNPs with 40 mol % cholesterol, in PBS and in 10%, 50% and 90% FBS over the course of 48 h. Stability is determined by measuring the absorption at 824nm at each timepoint relative to the absorption (824nm) at time t=0. Asterisks denote statistical significance (Student's t-test, p-value < 0.05).
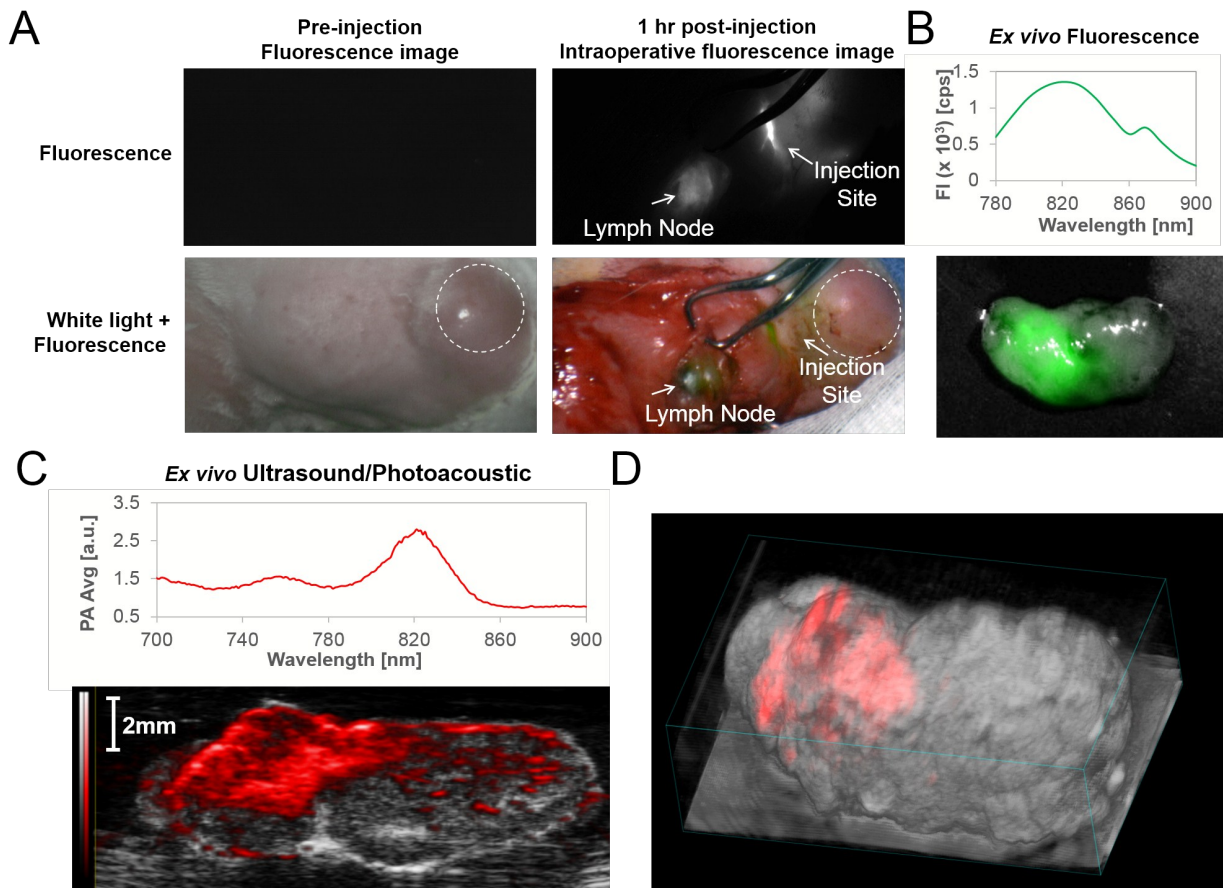
Fig. 5. Intraoperative imaging and resection of metastatic lymph node tissues from a VX-2 tumor-bearing rabbit. (A) Intraoperative fluorescence imaging showing both the fluorescence and white light/fluorescence images of the VX-2 buccal tumor and lymph node area before and 1hr after intradermal injection of JNPs. Dashed circle denotes the tumor area. (B) Fluorescence hyperspectral imaging of excised lymph node and associated fluorescence spectra of tissue, corresponding to JNPs. (C) Conformation of JNP signal spectra by photoacoustic imaging (top) and cross section of lymph node showing signal at 824nm (red). Photoacoustic signal is overlaid with B-mode ultrasound Scale bar represents 2 mm. (D) 3D rendering of photoacoustic/ultrasound image slices of lymph node, with accumulated JNPs rendered in red. Photoacoustic signal at 875nm is subtracted from 824nm to eliminate the contribution of hemoglobin to the photoacoustic signal.